Two-Photon Enhancement in Organic Nanorods[†]

Jeffery E. Raymond,[‡] Guda Ramakrishna,[‡] Robert J. Twieg,[§] and Theodore Goodson III*,[‡]

Department of Chemistry, Macromolecular Science and Engineering, Gerald R. Ford School of Public Policy, University of Michigan, Ann Arbor, Michigan 48109, and Department of Chemistry, Kent State University, Kent, Ohio 44242

The nonlinear optical response in one-dimensional organic nanorods of *N*,*N*-dimethyl-4−4((4-(trifluoro-methylsulfonyl)phenyl)ethynyl)aniline (DMFSPA) was investigated to probe the long-range interactions in the nanocrystals on the microscopic level. Differences in the linear and nonlinear optical properties are shown for two different morphologies of these organic crystals as well as for the chromophore in solution. The optimized nanocrystalline suspension had more than an order of magnitude increase in the two-photon excited fluorescence when compared to the solution phase of DMFSPA at similar chromophore densities. The one and two-photon properties of the nanocrystals and bulk crystals are compared by near-field scanning optical multiscope imaging. The images also provide insights into the formation of the nanorods during initial crystallization, changes in the optical response of the system with time, and the viability of these and similar nanomaterials for consideration in solid-state organic device applications. In addition to providing an imaging regime by which to assess this and other solid-state nanocrystalline organics, our investigation provides a simple and elegant method for enhancing the nonlinear optical response of organic materials by transition to nanoscale morphologies, without the need for additional chemical modification or synthesis.

1. Introduction and Background

Many methods have been investigated for the generation of nanowires and nanorods from inorganic materials,[1] while fewer avenues remain available for the formation of nanoscale solids consisting of purely organic materials. This detracts from the number of applications organic materials might be used for and limits the degree to which an organic fluorophore may be tuned without chemical modification to the molecule. It has recently been shown that small donor-π-acceptor molecules can be readily formed into one-dimensional (1D) nanocrystals via a simple, two-solution regime.[2] We show here that a rigid organic charge-transfer molecule, *N*,*N*-dimethyl-4−4((4-(trifluoromethylsulfonyl)phenyl)ethynyl)aniline (DMFSPA) (Figure 1a), can be crystallized into either 60 or 250 nm diameter nanorods (Figure 1b), enhancing the one- and two-photon optical response of the system. The linearity and regularity of the individual rods is an indication of their single crystal nature, primarily 1D growth mechanism and phase stability both in suspension and at ambient atmospheric conditions.

While there are many factors that are important to the enhancement of the two-photon cross-section of a molecule, a system's macromolecular geometry has played a large role in most recent accounts of organic materials assessed for this purpose. Through the use of branched, cyclical, charge-transfer, and two-dimensional organic molecules, it has been shown that a variety of molecular architectures provide reasonable avenues for producing functional nonlinear optical (NLO) materials.[3–5] Two-photon cross-section enhancement in these systems can be attributed to a variety of factors such as extended π-electron systems, bond-order-alternation, exciton delocalization, multi-directional dipole enhancement and control of symmetry.[4–8] Concurrently, increasing exciton hopping and decreasing thermal degradation pathways has been shown to provide enhancement to a materials two-photon excited fluorescence (TPEF) by way of an increased fluorescence quantum yield.[5,7–9] Unfortunately, these materials often require special and sometimes cumbersome synthetic regimes in their generation. In an attempt to gain some of the benefits of these larger architectures and longer range effects, we propose a transition to the solid-state to induce dipole-lattice interaction that will enhance our TPEF. The vast majority of the TPEF studies on these molecular architectures have been done in the solution phase, leaving some question as to their viability for solid-state device applications. We address this by crystallizing a small liquid crystalline organic charge-transfer molecule from the solution phase into nanorods, thereby providing a regime by which any linear donor-π-acceptor molecule might see its NLO properties enhanced and its potential for application increased. In contrast to a general decrease in fluorescence normally seen in bulk crystals, a drastic TPEF increase was seen in the resultant nanorod suspension that appears to function by a different route than typical J-type aggregate response.

Enhancement of the TPEF of rigid organic donor-π-acceptor molecules by increasing their intermolecular electronic interactions in the nanoscale solid state, producing high local fluorophore concentrations and increased dipole moments, makes this type of nanorod particularly attractive for a large number of applications.[3–6] Solid-state TPEF is often diminished when compared to the fluorescence of a solution phase D−A fluorophore if crystal dimensions are on the order of magnitude of tens of microns or larger. This happens for a variety of reasons, such as reabsorption, reflection, diffraction, etc. However, for crystals with dimensions at the nanoscale, many of these issues are minimized or eliminated altogether.

† Part of the "Larry Dalton Festschrift".
* To whom correspondence should be addressed. E-mail: tgoodson@umich.edu.
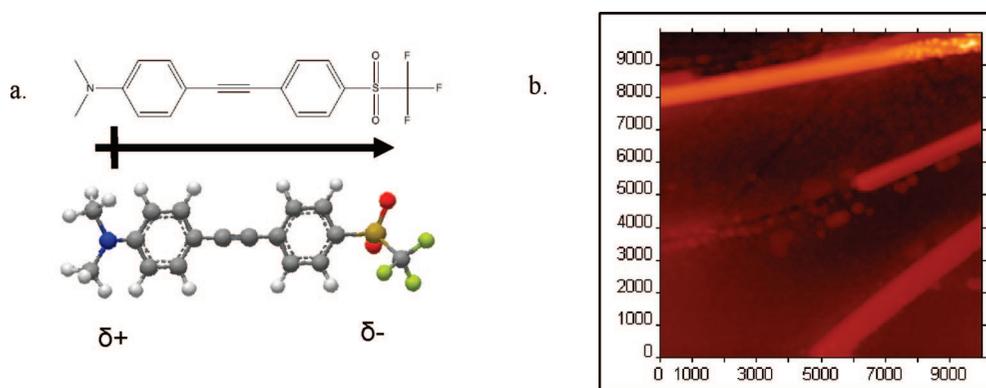‡ University of Michigan.
§ Kent State University.

Figure 1. Molecular model and nanorods of DMFSPA. (a) The charge transfer molecule DMFSPA. (b) AFM image of nanorods from preliminary DMFSPA nanocrystallization. Diameters range from 300−800 nm with aspect ratios near 30. Units are in nanometers.

In this paper, we report a system that shows increased quantum yield and two-photon cross-section upon formation of nanorods in suspension. While the electronic structure and excited states of similar molecules have been investigated previously,[6,8,9] the solid-state TPEF enhancement of these systems has not been shown or imaged. The nanorod samples were imaged by a near-field scanning optical multiscope (NSOM), allowing for topographical imaging by atomic force microscopy (AFM). Fluorescence was simultaneously observed qualitatively by near-field fluorescence optical microscopy (FOM) and near-field two-photon fluorescence microscopy (2PFOM).

2. Experimental Section

2.1. Crystallization. The crystallization of all samples was done by addition of a tetrahydrofuran (THF) solution of the molecule to water under ambient conditions. For the 60 nm diameter rods, 100 μL of a 407 μM THF solution was added to 4.9 mL of water, generating a suspension with a chromophore density of 8.14 μM. In the case of the 250 nm diameter rods, 400 μL of a 102.9 μM THF solution was added to 4.6 mL of water, generating a suspension with a chromophore density of 8.13 μM. Magnetic stirring occurred for one minute on addition of the THF solution. No precipitation was observed and filtration was not used.

2.2. NSOM Sample Preparation. Solutions and suspensions were applied dropwise to acid-cleaned glass slides in a spin coater. Samples were then subsequently subjected to vacuum for 3 min to remove all solvent.

2.3. Imaging. Images were obtained by use of a CDP MoScan NSOM multiscope. All AFM images are from non-contact mode. All NSOM and fluorescence images have excitation wavelength given. All image collection wavelengths (where applicable) are at 560 nm. Scales are given in nm.

2.4. Steady-State Measurements. All compounds were used as received without further purification. Measurements on solutions were carried out in spectroscopic grade tetrahydrofuran (THF) purchased from Sigma-Aldrich. Measurements on suspensions were carried out in THF/water mixtures (ratios are indicated). All water used was ultrapure (type I) from a Millipore filtration system. For the time dependent quantum yield study, absolute quantum yield was not obtained and only relative values are given.

2.5. Two-Photon Absorption Cross-Section Measurements. To measure the two photon absorption cross-sections, we followed the TPEF method. The details of the lasers and optical setup have been described elsewhere.[10] A 117 μM Coumarin 307 (Acros Organics) solution in methanol was used as the reference for the entire study. Quadratic dependence of TPEF intensity on input intensity was ensured at every wavelength. Two-photon cross-sections are calibrated to account for sensitivity of the photomultiplier tube (PMT) at the collection wavelengths of both the standard and the samples.

3. Results and Discussion

3.1. Steady-State Properties. For organic charge-transfer aggregate systems, there is a tendency to refer to the systems studied in terms of there photochemical response, even when implicit crystallographic information has been obtained. The standard model used for these systems was first provided by the historical paper by Kashi et al.[11] and is primarily concerned with two types of interactions in a two molecule system, H-aggregation and J-aggregation. This description of associative dimerization provides a general method for assessing the intermolecular electronic interactions effect on absorption and emission properties of the system. The H-aggregate model assumes that the dipoles associate in a side-to-side manner and is often characterized by stronger $\pi-\pi$ interactions, blue-shifted excitation, and a decreased fluorescence response due to excitation to a nonemissive triplet state. In contrast, J-aggregate behavior is characterized by a head-to-tail dipole association, and its strongly enhanced dipole moments lead to greater exciton delocalization, red-shifted excitation, and an increased fluorescence response for the system. While this is a good starting point for discussion of aggregate systems, it cannot and should not be used to implicitly describe aggregate systems of many molecules. Rather, it is more useful to use these models for description of extended dipole network behavior. Crystalline structures, by their very nature, demand some component of both types of interaction for these materials, and one cannot readily isolate response to a two molecule system. Therefore, it is more appropriate to discuss the H-type and J-type response of the system, keeping in mind that the system under investigation by necessity possesses both types of interactions, and that these descriptions are purely in reference to electronic transitions of the system governed by both short and long-range interactions.

The optical absorption and fluorescence results for the DMFSPA solution and a nanorod suspension are given in Figure 2. Similar absorption intensities for the two samples stand in sharp contrast to the large fluorescence enhancement in the suspension sample. As will be discussed later, this is primarily due to a 10-fold increase in the quantum yield upon nanocrystallization. Both sets of spectra are normalized to the larger peak for clarity and have concentrations of 12.4 μM. The shift in the absorption maxima from 394 nm for the solution to 364 nm for

Two-Photon Enhancement in Organic Nanorods

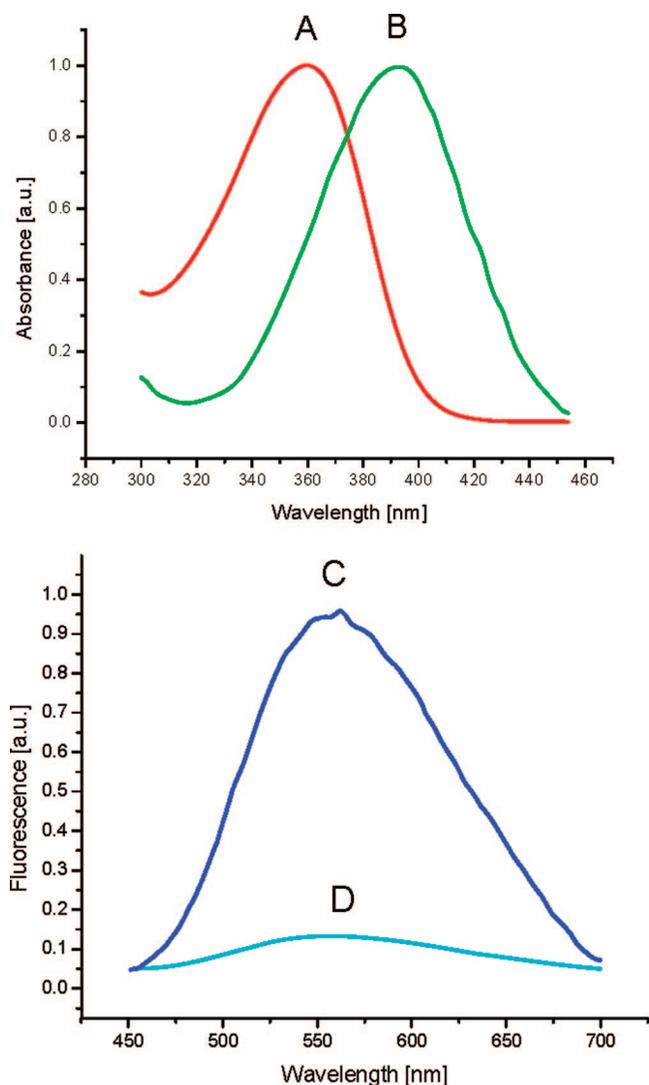*J. Phys. Chem. C, Vol. 112, No. 21, 2008* **7915**

Figure 2. Steady state absorption and emission spectra for the suspension and solution phase DMFSPA. (A) Absorbance for 250 nm rod suspension in 8% THF. (B) Absorbance for solution phase. (C) Fluorescence intensity for 250 nm rod suspension in 8% THF. (D) Fluorescence intensity for solution phase.

the nanorod suspension would typically imply the generation of a nonemissive H-type aggregation response.

Falling within the general umbrella of aggregation-induced emission (AIE),[12–15] this sort of response is characterized by a dual emissive kinetic model in which the lattice interactions with the molecule allow a generally nonemissive excited triplet state to readily transition to a more emissive state,[14,15] making H-type absorption response in the system potentially more fluorescent than J-type response. Several organic systems have been shown to exhibit this type of 1P response, showing increased AIE with transition to smaller and smaller crystals.

Morphologies in nanoscale charge transfer systems depend on solvent selection, molecular architecture and dipole number/ strength. For rigid donor-π-acceptor systems like ours, with accessible regions of aromatic groups, there is little chance that aggregate structures could be formed purely from $\pi-\pi$ stacking or from dipole$-$dipole interactions alone. It is therefore necessary to think of DMFSPA nanorods, as mentioned above, as possessing both H-type and J-type character simultaneously, though certainly from a photochemical perspective one may be seen to dominate. Though a strict evaluation of the implicit crystal structure for the nanocrystalline and bulk materials

studied is beyond the scope of the study presented here, it should be noted that other linear charge transfer molecules displaying primarily H-type excitation still possess a dipole dominated growth mechanism and have been shown by X-ray diffration to possess dipoles primarily oriented in the direction of growth.[13,16,17] This is presumed to be the case for our systems and is supported to a degree by imaging presented later in this study.

In addition to the local environmental enhancement generated by a regular array of dipoles, our molecule possesses a "rotorlike" component in its dimethylaniline donor group. Other studies on AIE have shown that locking the rotation of such groups in D$-$A systems where small organic molecules have assembled in suspension give increased fluorescence response.[12,15,18,19] This effect is attributable to (1) a decrease in the availability of nonemissive excited-state vibrational relaxation and (2) a more rigid architecture that allows the donor electron pair to more fully contribute to charge transfer in the molecule.

The gross increase in emission intensity and blue-shift in absorption for the nanorods studied, when compared to the solution, is an indicator that there is greater exciton delocalization, generation of a triplet state accessible lattice induced emissive state, and lower opportunity for thermal degradation of the excited state in the nanocrystalline phase molecules. A complete overlay of the absorption/emission data shows that the bulk, nanorod, and solution phase samples show clearly that each sample possesses a different excitation and relaxation regime that we attribute to differing intermolecular interactions.

3.2. Time-Dependant Quantum Yield Measurements. A significant change in absorption spectra, emission intensity and, consequentially, quantum yield was seen during the growth of these nanostructures with efficiency closely tied to THF concentration and suspension age. Figure 3 shows the absorption spectra over time for two different solutions with relative quantum yields at pertinent times for the processes listed. The sample that generated the 60 nm rods, 2% THF, shows a lower loss of ε and η from aging than that of the 250 nm rod sample. The quantum yield from the 8% THF, 250 nm rod sample increases from 42% of maximum initially to a maximum efficiency at 3 min. The quantum yield of the 250 nm rod suspension then decreases significantly to a value of 19% of maximum 30 min after formation. In contrast, a maximum quantum yield is seen in the 60 nm rods at 1 min with constant and less dramatic decrease in quantum yield over time giving a quantum yield of 73% of maximum after 30 min. From these results, it can be taken that lower concentrations of "good" solvent, THF, allows for faster crystallization and longer retention of higher quantum efficiency nanocrystals. The images shown in Figure 4 display a complimentary aging study of the suspension by NSOM/AFM. Observing the rods five minutes after crystallization onset (Figure 4a$-$c), it is clear that the nanorods are single crystals with diameters of 250 nm and lengths greater than several microns. The NSOM image (Figure 4b) shows the presence of metastable "protorods" having spherical structures with diameters of approximately 60 nm. On several of the rods, these spheres can be seen attached to the rod ends, confirming a 1D growth mechanism requisite of rodlike morphologies at these scales. Further aging shows reduction in these "protorods" and continuous rod$-$rod aggregation. Note that, though the individual rod dimensions remain the same, the rod$-$rod aggregation size increases continually during this time. The 2PFOM image displayed for the youngest sample (Figure 4c) was generated by 840 nm excitation. By its very nature, the 2PFOM image of these
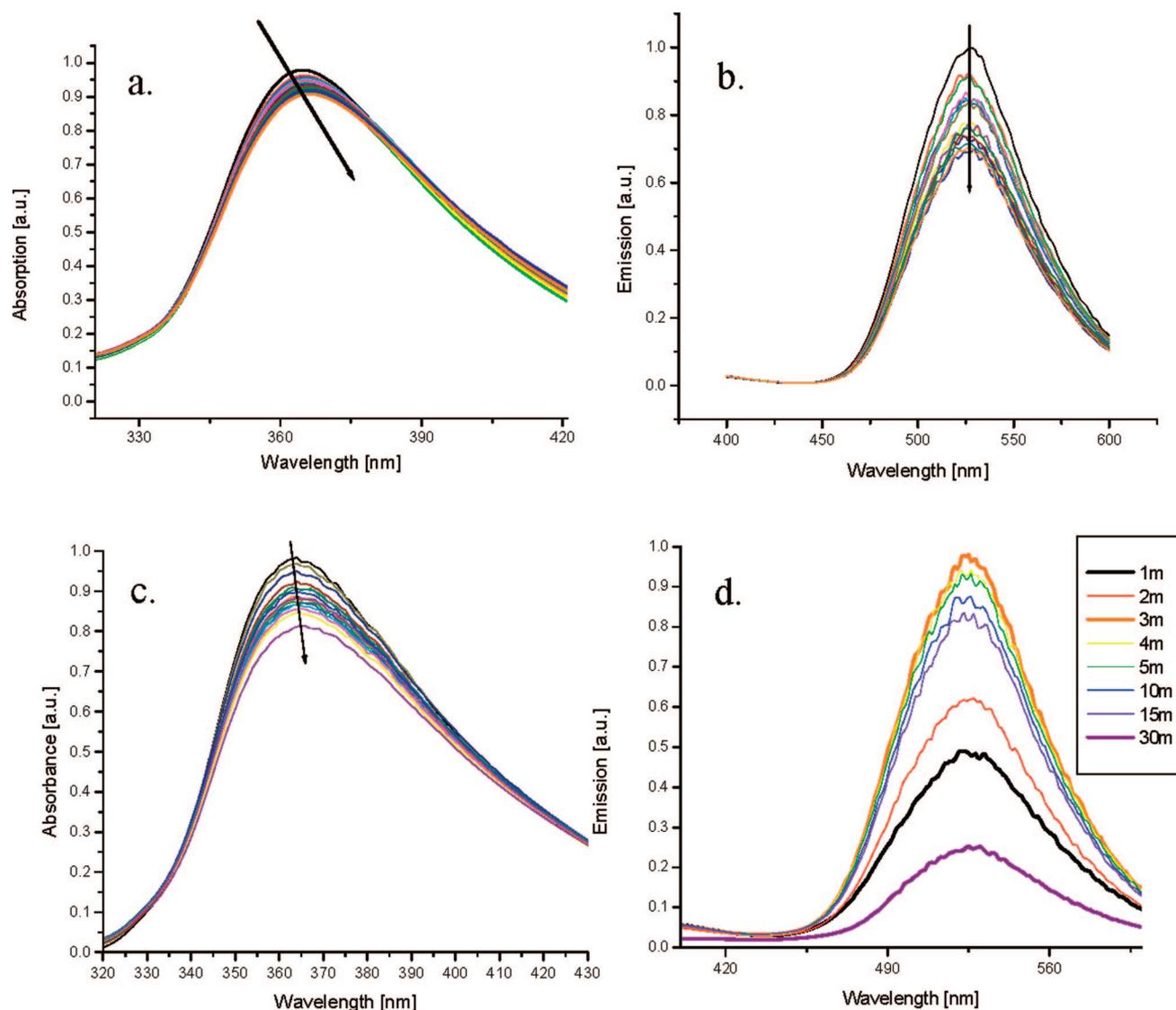
Figure 3. Absorption and emission spectra for the two characterized rod samples aging over 30 min. (a) Absorption, 60 nm rods. (b) Emission, 60 nm rods. (c) Absorption, 250 nm rods. (d) Emission, 250 nm rods.

systems is limited by the TPA cross-section, quantum yield of the sample, and the quadratic relationship between 2P fluorescence and incident light intensity. Typical 2PFOM imaging is performed on samples with cross-sections that are 2 to 3 orders of magnitude greater than the 250 nm rod samples with features sizes several times larger than the diameter of the observed rods. Despite these factors, the clear contrast at the rod locations is further indication of this system's robustness for evaluating organic two-photon fluorescent nanomaterials and correctly correlating emission with specific morphologies and nanostructures within a sample. The rods appear to bundle with advancing age, while the basic morphology and dimensions of the rods do not change, implying no further change in crystal structure and that the rod−rod aggregation is largely a surface−surface interaction between rods. Over time, it can be seen that the loss of quantum efficiency can be attributed to the aggregation/bundling of the rods with each other and not additional growth of the crystals or transitions to different morphologies.

3.3. Two-Photon Measurements. Two-photon excited fluorescence is a third order nonlinear process in which the fluorescence intensity is related quadratically to the excitation intensity. The two-photon cross-section is therefore a higher order analog to the single photon absorption phenomenon related to the molar extinction coefficient of a material. Two-photon

absorption benefits from being a process that uses less energetic photons and is typically enhanced by processes that increase a species' quasi-excited-state lifetime and allow for greater exciton delocalization.

To fully assess the TPEF enhancement seen in the nanocrystalline samples, it is critical to characterize the molecule in solution as well as in the nanorod suspensions. Table 1 provides a summation of the absorption and emission spectra for the samples studied and shows a two-photon emission maximum near 525 nm for the 60 nm rod sample. This is a 35 nm blueshift from the 1P emission. In contrast, the absorption maximum for the excited state allowed in the 2P excitation is lower energy than the 1P allowed excitation. These findings are in keeping with the dual emissive kinetic model, showing that the allowed 1P transition and 2P transitions are different but are provided similar lattice-induced energy levels that make a typically nonemissive excited state emissive.[13,20] The TPEF blue-shift is diminished in the larger rod sample with the 250 nm rods having a 30 nm emission blue-shift and the solution phase, giving only a 20 nm shift. This type of effect has been seen in other organic aggregate systems[12,13,18,20,21] and implies an increased Coulombic interaction of the molecule with its environment, which is the crystal lattice of the nanorod in the rod samples. This means that the two-photon emissive state is even more energetic for
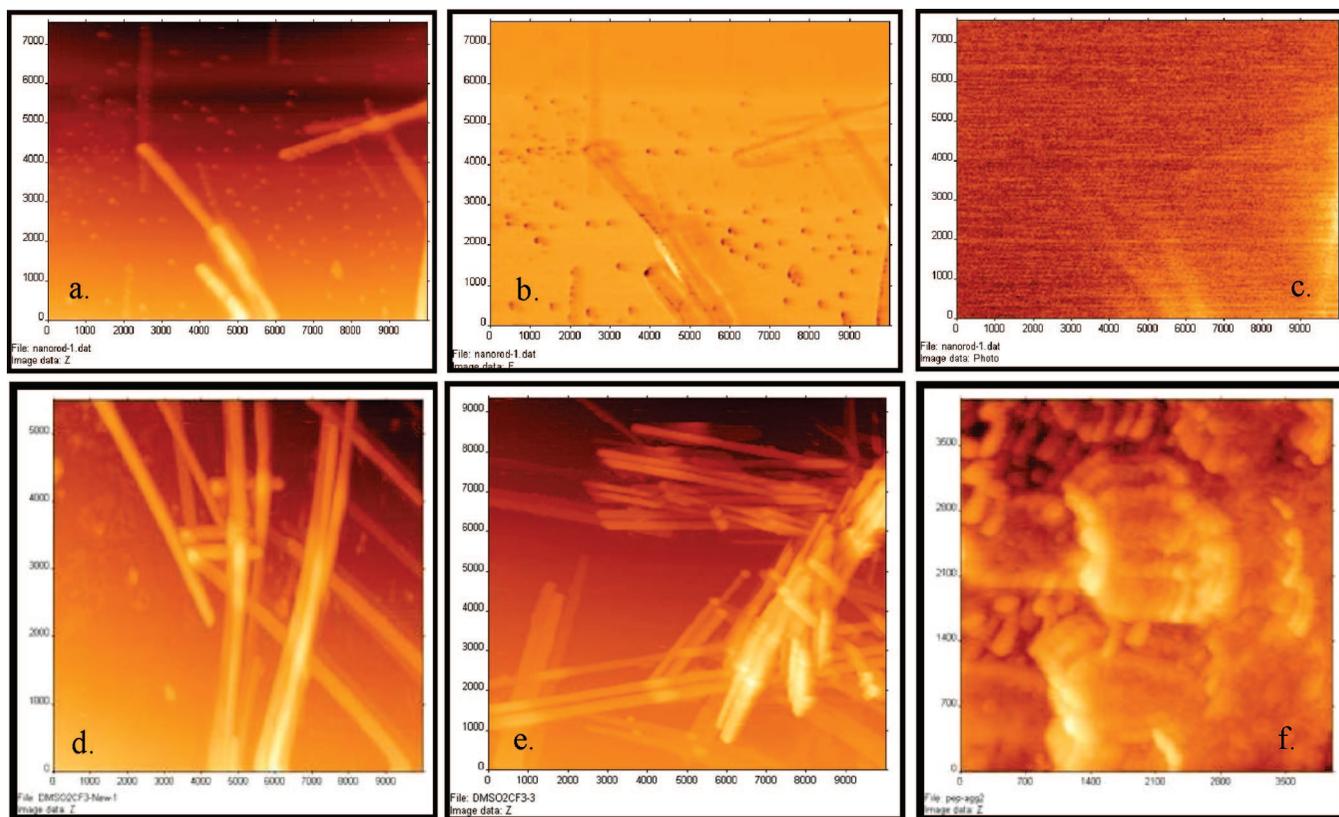
Two-Photon Enhancement in Organic Nanorods

J. Phys. Chem. C, Vol. 112, No. 21, 2008 **7917**

Figure 4. Quantum yield time study images. (a) AFM, (b) NSOM, and (c) 2PFOM images of a 250 nm rod sample 5 min after crystallization. Subsequent AFM images of the same sample (d) 30 min, (e) 4 h, and (f) 48 h after crystallization. Scales are in nm.

TABLE 1: Relative Spectra Peaks for Sample Systems

sample	1P absorption maximum	1P emission maximum	1P Stokes shift	2P absorption maximum	2P emission maximum	change in emission; 1P → 2P
THF solution	394 nm	560 nm	166 nm	840 nm	540 nm	20 nm
250 nm rods	364 nm	560 nm	194 nm	840 nm	530 nm	30 nm
60 nm rods	364 nm	560 nm	194 nm	840 nm	525 nm	35 nm

TABLE 2: Optical and Nonlinear Optical Properties for the DMFSPA Samples

sample	solution phase	250 nm rods	60 nm rods	"aged" 60 nm rods
solvent	THF	23:2 water to THF (8%)	49:1 water to THF (2%)	49:1 water to THF (2%)
concentration	9.23 μM	8.23 μM	8.14 μM	8.14 μM
sample age	n/a	5 min	5 min	48 h
ε (mol^{-1}cm^{-1})	$2.02 * 10^4$	$2.00 * 10^4$	$6.34 * 10^4$	$0.74 * 10^4$
η	0.006	0.056	0.049	0.041
δ (GM)	90	99	419	84
$\eta * \delta$ enhancement	n/a	10.3 times	38 times	6.4 times
aspect Ratio	n/a	~25	~15	~15

the rods and is closer in energy to the initial excited-state than in the solution. A summary of the TPEF materials investigated is given in Table 2 and details the TPEF enhancement in the suspension in an implicit manner. For our most emissive sample, the 60 nm rods, the emission was enhanced close to 40 times that of the solution phase per chromophore.

It is important to note that both the quantum yield and the two-photon cross-section for the 60 nm rod sample decrease with aging. From the earlier images shown in Figure 4, it can be seen that the only difference between the rods at their highest quantum yield and later "ages" is their aggregation level. The rod size and morphology does not change with time, and the material is not chemically changed. Changes in quantum yield and two-photon absorption are therefore largely attributable to the aggregation. The same decrease in optical response seen with crystal defects in larger assemblies (i.e., dislocations,

defects, reabsorption, etc.) is emulated by this process. Each point of contact made between rods may then be thought of as a small disturbance, disrupting the same organization that was responsible for the increased optical response of the system. The intermolecular electronic communication that helps to further enhance the dipole of these molecules can be thought of as "quenched" at these contact points, decreasing both quantum yield and two-photon cross-sections as the available avenues for exciton delocalization, as well as increasing the number of thermal degradation pathways through interaction with additional surfaces and a general decrease in the dipole-lattice interactions.

The end result of these enhancements in the 60 nm diameter rods of these molecules is an overall 38 fold increase in the TPEF of this material with the benefits of crystallization decreasing with time. The 250 nm rods also show a considerable
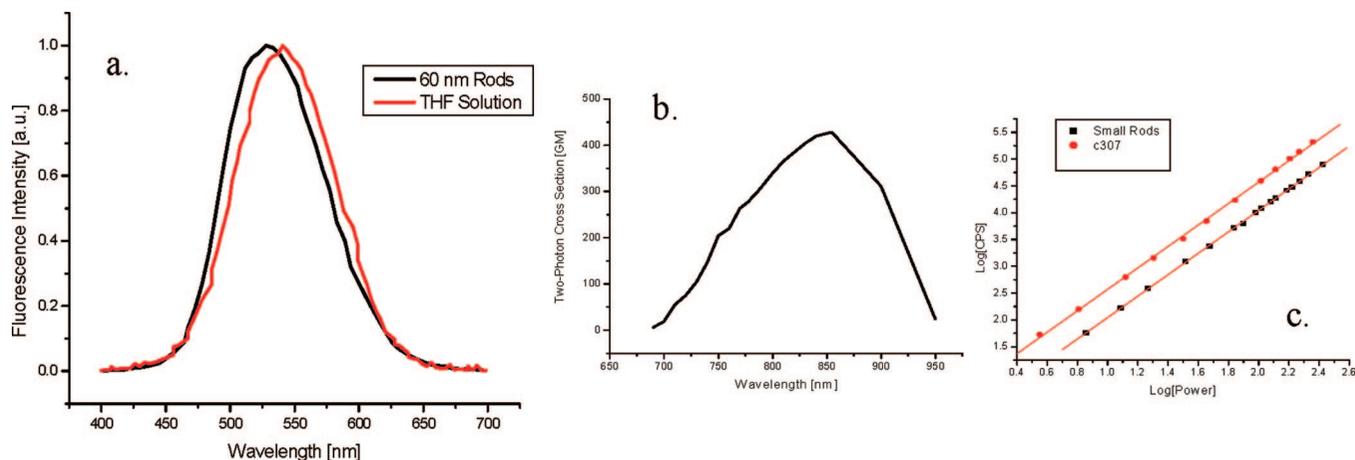
Figure 5. (a) Two-photon emission spectra contrasting the 60 nm rod suspension to the solution sample. (b) Two-photon cross-section spectra of the 60 nm rod suspension, typical of all samples studied. (c) Graph depicting the quadratic relationship of the 60 nm rod samples two-photon excited emission, dependent on excitation intensity at 840 nm.

increase of 10 times the TPEF of the solution phase. The two-photon emission (Figure 5a) and cross-section (Figure 5b) spectra for the 60 nm rod are comparable to the other samples studied with slightly lower emission wavelength for the 250 nm rods and the solution phase molecule. The TPEF enhancement of the rod samples is attributed to further polarization of the molecular dipoles by the regularly ordered and partially charged environment that the nanocrystal provides. The regular network of dipoles induces additional exciton delocalization, increasing the two-photon cross-section marginally for the 250 nm rod samples and grossly in the 60 nm rod samples. The quadratic relationships between the incident and the emission intensity for the 60 nm rods is shown representatively for the samples and is demonstrated in Figure 5c to confirm the optical process as nonlinear.

A decreased two-photon cross-section is reported for the aged rod sample (Table 2) in addition to a decrease quantum yield and molar extinction coefficient. As stated previously, we attribute this decrease to excessive aggregation (similar to that shown in Figure 4f) and solvent trapping in bundle cavities. The 250 nm rod sample has both a lower ε and two-photon cross-section when compared to the 60 nm rod sample, at similar chromophore concentrations. We propose that this enhancement is lower for the 250 nm rods due to a less emissive core. An argument for this will be detailed more fully in the following section.

3.4. Imaging. The viability of use of an NSOM multiscope for confirming our crystallization regime is readily shown (Figures 1 and 4). The NSOM/AFM/FOM images generated simultaneously provide further confirmation of the curvature of sample features, regardless of depth of field. Although for this study FOM and 2PFOM does not help with dimensional analysis, the contrast between emissive and less emissive materials can be seen. These imaging methods were critical to determining the cause of the quantum yield decrease with time and explaining the differing emission behavior for the two rod samples.

When the incident intensity and collection times for FOM imaging of the rods were drastically increased and the excitation intensity was decreased, a stark contrast between the two samples was observed. Noting the images in Figure 6, we see that the emission from the 250 nm rods comes primarily from the outermost region of the sample, indicated by "edge" illumination. When fluorescence intensities are sampled radically across the rods and compared to integrations for a disk in the

60 nm rod sample and a ring in the 250 nm rod sample. The superimposed integrations use radii and ring thicknesses equal to the penetration depth for this material (31 nm). The comparison shows clearly that there is good correlation between the proposed interaction depth and the actual fluorescence response. Excitation for both images is at 370 nm, and fluorescence collection occurs at 560 nm.

Though spectroscopic data indicates a highly aligned nanocrystalline system with strong dipole coupling, an initial study was done to confirm that our system did in fact respond differently to different polarizations of light (Figure 7). An arbitrary polarization was used for Figure 7a.2 and a polarization 90° from that was used for Figure 7b.2. Note that the "top" rod provides the majority of the emission in the parallel (a) image and that the "bottom" rod provides the majority in the perpendicular (b) image. From this, it can be taken that the associated rods have primary dipole moments that are uniform over each rods structure and positioned in opposite directions to each other in real space. Figure 7c shows an aged sample in which a rod bundle that appears to be "under" the other structures in the AFM image but provides the highest emission in the FOM image. Figure 7c,d was taken using a slightly different polarization regime in which emission was first maximized by changing the polarization of the excited light. Figure 7c.2 shows the parallel, maximum detection, "on" state for the observed bundle. In contrast, Figure 7d.2 was taken using light perpendicular to the maximum, giving a "off" response from the bundle. The emission intensity scales have been left for both panels c and d images to show that the bundle emission in panel c is several times more intense than the background intensity. It can also be seen that the bundle intensity of the image in panel d is not detectable above background and that the background for both images are the same.

For less regular crystallizations, generating various sizes and morphologies in the resultant crystals, it takes little imagination to anticipate its use in the determination of the most emissive products. This becomes particularly useful when considering materials that display TPA response. The generation of just a few strongly emissive morphologies in the presence of low emission structures may give a false indication of the response of system components that should be evaluated separately. Similarly, self-quenching materials, such as H-aggregates, may induce lower emission in adjacent materials. Figure 8 shows a sample that was agitated by sonication during crystallization. This product showed ab-
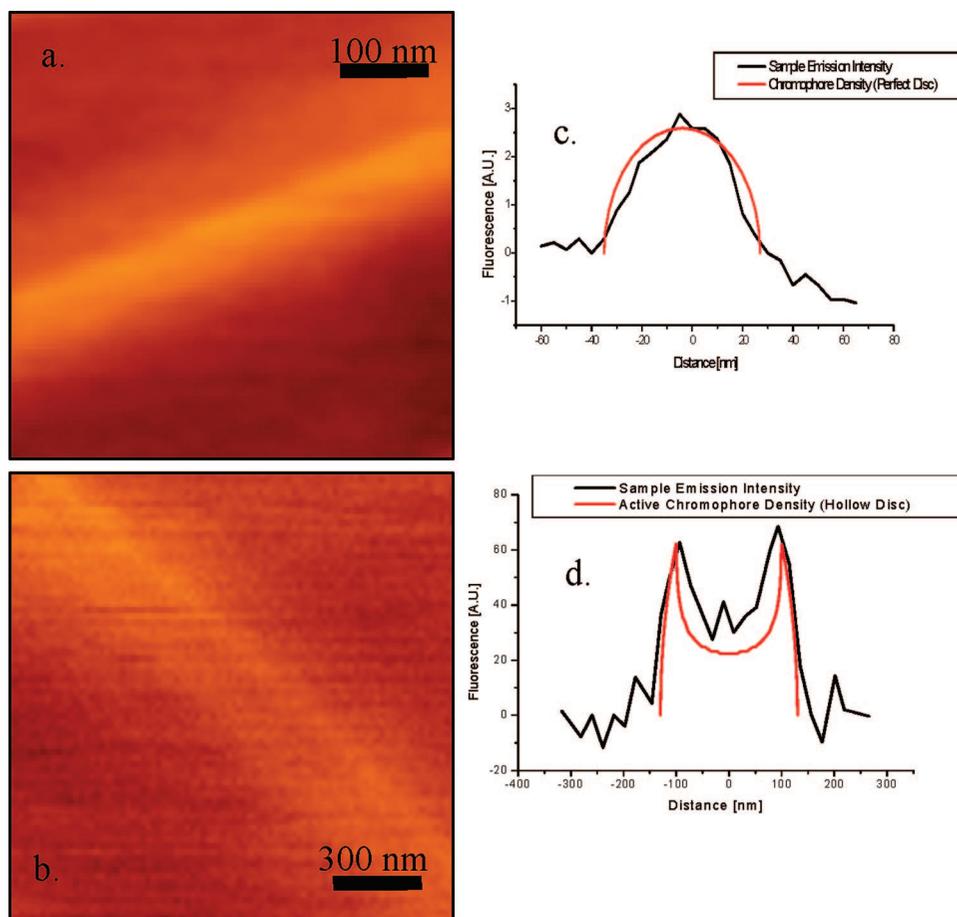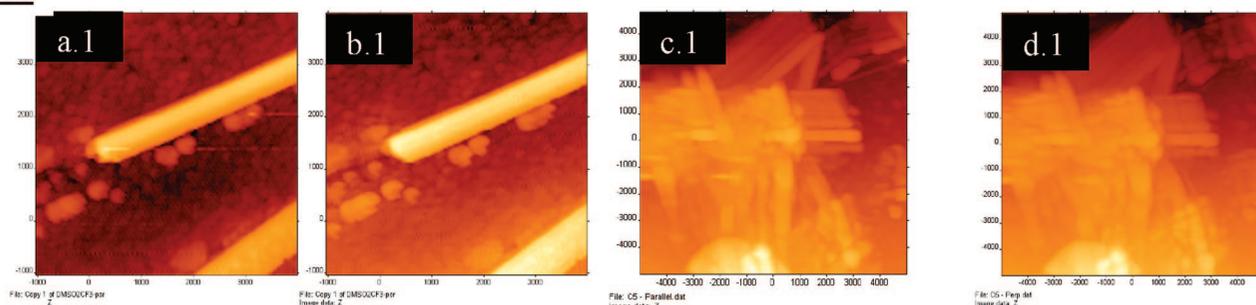
Two-Photon Enhancement in Organic Nanorods

J. Phys. Chem. C, Vol. 112, No. 21, 2008 **7919**

Figure 6. The 60 nm rod (a) shows a more homogeneous emission. The 250 nm rod (b) shows surface emission, characterized primarily by "edge" illumination. A line graph of the fluorescence intensities for the 60 nm (c) and the 250 nm (d) sample show good correlation to disk and thick ring models, confirming that only the outer region of the 250 rods participate in fluorescence.
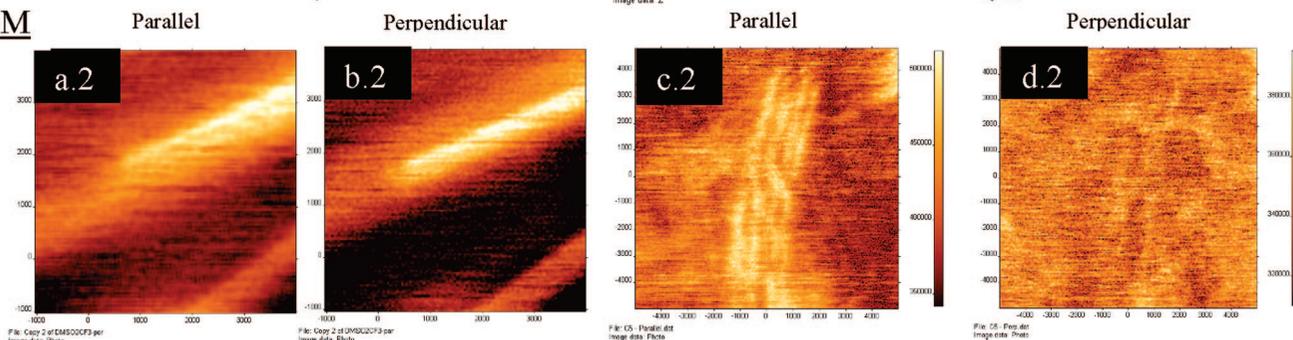

Figure 7. Polarized FOM Imaging of 250 nm Diameter Rods. Both the AFM image (1) and the FOM image (2) for each scan is provided to be certain that the exact same features were imaged in for both polarizations of light. Images (a) and (b) show a two rod system, stacked and off-set as indicated in the AFM image. Images (c) and (d) show a collection of rod bundles formed after 24 h of suspension.

sorption similar to the nanorod samples but displayed only nominal emission. Images of the sample show that the product was a combination of nanorods and spheroids. The FOM image shows clearly that the spheres show no emission at the collection wavelength and may in fact be reabsorbing at the detection wavelength.
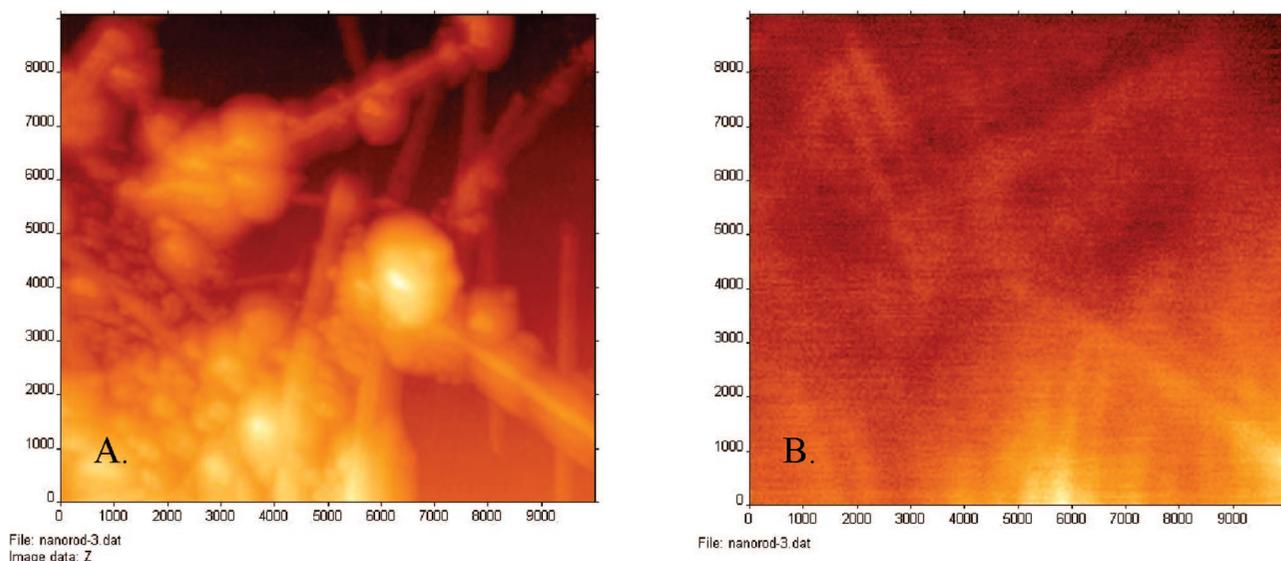
Figure 8. The low emission sonicated rod sample shows two general morphologies in AFM mode (A). FOM imaging shows that the rod morphologies in the sample remain emissive (B). Negative contrast for areas containing high concentrations of the spherical morphologies show the nonemissive nature of the structures and their ability to inhibit rod fluorescence in their vicinity. Excitation wavelength is 370 nm.
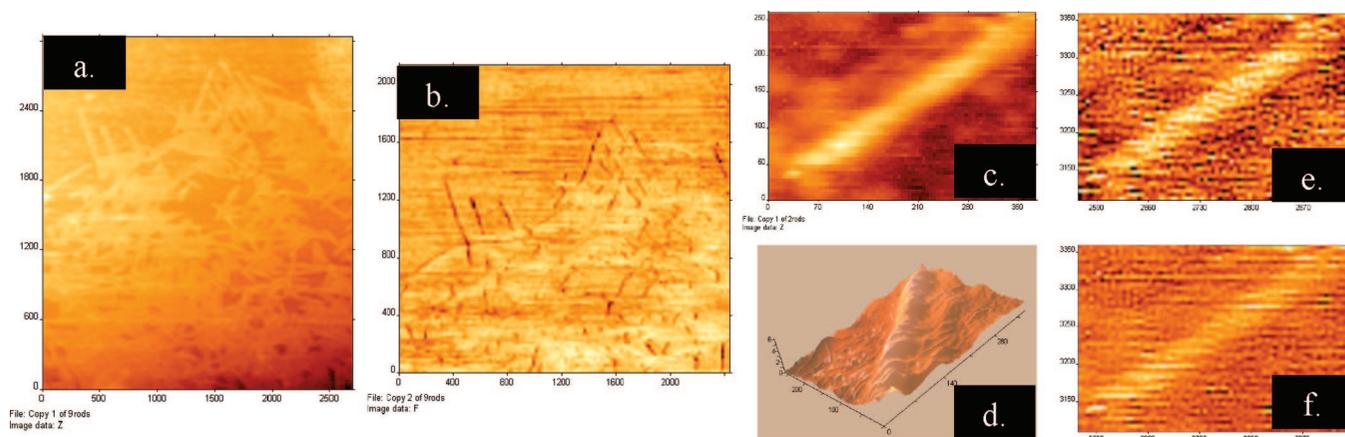

Figure 9. (a) AFM and (b) NSOM images of a one hour old sample for the 60 nm rod sample characterized. Note that the NSOM image is generated with incident light at the two-photon cross-section maximum of 840 nm. (c) Isolation of a lone rod shows both dimensionality and curvature when the noncontact AFM image is viewed in a three-dimensional rendering (d). The 2PFOM image of the isolated rod (e) is provides significantly more signal (∼4 times) when twice the excitation intensity is provided (f).

Though the resolution for noncontact AFM is lower than more invasive imaging methods, the images of the 60 nm rod samples (Figure 9) clearly show that it is sufficient for resolving crystal features at this scale. Isolation of a single rod indicates that both curvature and dimensions can be resolved using this method for confirmation of nanostructure. Furthermore, it allows the viewing of structures by several complimentary methods simultaneously, ensuring that the same sets of features are being observed both topographically and optically. Resolution of features less than 20 nm can be difficult to obtain and confirm for both noncontact mode AFM and NSOM imaging. Here, the resolution provided by use of longer wavelength near-field optical response allows confident differentiation of structures at this level and provides information critical to correlating morphology to optical response. The structure observed in Figure 9c was also imaged by TPFOM in a manner similar to Figure 7. However, instead of changing polarization, system input intensity was varied from 5.1 mW (Figure 8e) to 10.3 mW (Figure 8f) in two subsequent scans with collection times roughly 50 times longer than in regular FOM. While the background showed an expected increase of roughly two with doubling of the input intensity, the intensity of the rods showed

a 3.8 fold increase over background. This was calculated by subtracting the average background intensity from each image and comparing the intensity average along the axis of both rods. These images confirm that the primary mode of excitation occurring is nonlinear and not the result of a linear absorption-emission response; these images are some of the first two-photon images taken of isolated nanostructures that are not deposited in a composite thin film. Further refinement of this and similar imaging systems may make available an entirely new regime by which to study the NLO response of single nanocrystals in isolation.

4. Conclusion

By generating functionally enhanced NLO organic nanomaterials from a simple two-solvent method, this study opens the way for similar enhancement in other charge transfer systems with little or no additional wet chemistry. The molecular system studied showed unique 1P and 2P fluorescence enhancement on transition to the solid-state, showing absorption and emission properties typical of neither H- nor J-aggregates. The increase in quantum efficiency and two-photon cross-section with

Two-Photon Enhancement in Organic Nanorods

J. Phys. Chem. C, Vol. 112, No. 21, 2008 **7921**

properly controlled nanocrystallization leads to a total increase in the TPFE of this material close to one and half-orders of magnitude. In addition to this, the transition to solid state makes this type of sample preparation much more robust for thin-film impregnation applications. This solid-state transition is even more favorable when one takes into consideration that the functional lifetime of imbedded crystalline materials tend to be greater than similar quantities dispersed via solution in a polymer matrix, which is perhaps best exemplified in the difference between liquid crystal impregnated polymers with and without micelle formation.[22] This is particularly true for organic materials that have reactive functional groups, high potential for chelation, are prone to evaporation, or tend to phase separate. The normal drawback of a crystal dispersion, decreased fluorescent response, is therefore eliminated. AFM−NSOM−FOM imaging for analysis of donor-π-acceptor systems with nanoscale features has been shown in this study to be very illuminating when considering the size and stability of various morphologies.

References and Notes

(1) (a) Dick, K. A.; Deppert, K.; Larsson, M. W.; Martensson, T.; Seifert, W.; Wallenberg, L. R. *Nat. Mater.* **2004**, *4*, 380–384. (b) Kang, Z. H.; Wang, E.; Mao, B. D.; Su, Z. M.; Gao, L.; Lian, S. Y.; Xu, L. *J. Am. Chem. Soc.* **2005**, *127*, 6534–6535. (c) Ween, X. G.; Wang, S. H.; Ding, Y.; Wang, Z. L.; Yang, S. H. *J. Phys. Chem. B.* **2005**, *109*, 215–220.

(2) Zhang, X.; Zhang, X.; Zou, K.; Lee, C.; Lee, S. *J. Am. Chem. Soc.* **2007**, *129*, 3527–3532.

(3) Varnavski, O.; Yan, X.; Mongin, O.; Blanchard-Desce, M.; Goodson, T., III. *J. Phys. Chem. C.* **2007**, *111* (1), 149–162.

(4) Bhaskar, A.; Ramakrishna, G.; Hagedorn, K.; Varnavski, O.; Mena-Osteritz, E.; Bauerle, P.; Goodson, T., III. *J. Phys. Chem. B* **2007**, *111* (5), 946–954.

(5) (a) Ramakrishna, G.; Bhaskar, A.; Goodson, T., III. *J. Phys. Chem. B* **2006**, *110* (42), 20872–20878. (b) Bhaskar, A.; Guda, R.; Haley, M. M.; Goodson, T. G., III. *J. Am. Chem. Soc.* **2006**, *128* (43), 13972–13973.

(6) Varnavski, O.; Goodson, T., III.; Sukhomlinova, L.; Twieg, R. *J. Phys. Chem. B* **2004**, *108*, 10484–10492.

(7) Varnavski, O.; Leanov, A.; Liu, L.; Takacs, J.; Goodson, T., III. *J. Phys. Chem. B* **2000**, *104*, 179–183.

(8) Bhaskar, A.; Ramakrishna, G.; Twieg, R.; Goodson, T., III. *J. Phys. Chem. C* **2007**, *111*, 14607–14611.

(9) (a) Bhaskar, A.; Ramakrishna, G.; Lu, Z.; Twieg, R.; Hales, J. M.; Hagan, D. J.; Van Stryland, E.; Goodson, T., III. *J. Am. Chem. Soc.* **2006**, *128* (36), 11840–11849. (b) Twieg, R.; Ebert, M.; Jungbauer, D.; Lux, M.; Reck, B.; Swalen, J.; Teraoka, I.; Willson, C. G.; Yoon, D. Y.; Zentel, R. *Mol. Cryst. Liq. Cryst. Sci. Technol.* **1992**, *217*, 19–24. (c) Burland, D. M.; Miller, R. D.; Reiser, O.; Twieg, R. J.; Walsh, C. *J. Appl. Phys.* **1992**, *71*, 410–417.

(10) Schwahn, D.; Richter, D.; Lin, M.; Fetters, L. J. *Macromolecules* **2002**, *35* (9), 3762–3768.

(11) Kasha, M.; Rawls, H. R.; El-Bayoumi, M. A. *Pure Appl. Chem.* **1965**, *11*, 371–392.

(12) Hong, Y.; Dong, Y.; Tong, H.; Li, Z.; Haubler, M.; Lam, J.; Tang, B. *Proc. SPIE* **2007**, *6470*, 1–12.

(13) Bhongale, C.; Chang, C.-W.; Lee, C.-S.; Diau, E.; Hsu, C.-S. *J. Phys. Chem. B* **2005**, *109*, 13472–13482.

(14) Patra, A.; Anthony, S. P.; Radhakrishnan, T. P. *Adv. Func. Mater.* **2007**, *17*, 2077–2084.

(15) Li, Y.; Li, F.; Zhang, H.; Xie, Z.; Xie, W.; Xu, H.; Li, B.; Shen, F.; Ye, L.; Hanif, M.; Ma, D.; Ma, Y. *Chem. Comm.* **2007**, *3*, 231–233.

(16) Iyoda, M.; Hasegawa, M.; Enozawa, H. *Chem. Lett.* **2007**, *36*, 1402–1407.

(17) Sonada, Y.; Goto, M.; Tsuziki, S.; Tamoaki, N. *J. Phys. Chem. A* **2006**, *110*, 13339–13379.

(18) (a) Tong, H.; Dong, Y.; Hong, Y.; Haussler, M.; Lam, J.; Sung, H.; Yu, X.; Sun, J.; Williams, I.; Kwok, H. S.; Tang, B. *J. Phys. Chem. C* **2007**, *111*, 2287–2294. (b) Patra, A.; Hebalkar, N.; Sreedhar, B.; Sarkar, M.; Samanta, A.; Radhakrishnan, T. P. *Small* **2006**, *5*, 650–659.

(19) Tong, H.; Dong, Y.; Hong, Y.; Haussler, M.; Lam, J.; Sung, H.; Yu, X.; Sun, J.; Williams, I.; Kwok, H S.; Tang, B. *Chem. Comm.* **2006**, *2*, 1133–1135.

(20) (a) Zhang, W.; Cozzolino, A.; Mahmoudkhani, A.; Tulumello, M.; Mansour, S.; Vargas-Baca, I. *J. Phys. Chem. B* **2005**, *109*, 18378–18384. (b) Wang, H. Z.; Zheng, X. G.; Mao, M. D.; Yu, X.; Gao, Z. L.; Yang, G. Q.; Wang, P. F.; Wu, S. K. *Appl. Phys. Lett.* **1995**, *66* (1), 2777–2779. (c) Koren, A.; Curtis, M. D.; Francis, A. H.; Kampf, J. W. *J. Am. Chem. Soc.* **2003**, *125*, 5040–5050. (d) Qian, Y.; Li, S.; Zhang, G.; Wang, Q.; Wang, S.; Xu, H.; Li, C.; Li, Y.; Yang, G. *J. Phys. Chem. B* **2007**, *111*, 5861–5868. (e) Prakash, J. M.; Radhakrishnan, T. P. *Cryst. Growth Des.* **2005**, *5* (5), 1831–1836.

(21) Belfield, K. D.; Bondar, M.; Hernandez, F. E.; Przhonska, O. V.; Yao, S. *Chem. Phys.* **2006**, *320*, 118–124.

(22) (a) Schuck, P. J.; Willets, K. A.; Fromm, D. P.; Twieg, R. J.; Moerner, W. E. *Chem. Phys.* **2005**, *318*, 7–11. (b) Galvan-Gonzalez, A.; Belfield, K. D.; Stegeman, G. I.; Canva, M.; Chan, K.-P.; Park, K.; Sukhomlinova, L.; Twieg, R. J. *Appl. Phys. Lett.* **2000**, *77*, 2083–2085.